RESEARCH ON PRECISE GEOMETRY MODEL OF SYNTHETIC APERTURE RADAR INTERFEROMETRY

Song Shujing, Liu Yihua, Jiao Jian, Zeng Qiming

GIS and Remote Sensing Institute of Peking University, Beijing, China
qmzeng@pku.edu.cn, enorlae@gmail.com

KEY WORDS: InSAR, Geometry Model, DEM Correction, GCP

ABSTRACT:

InSAR, a new branch of Remote Sensing technology, has developed remarkably in recent years. Many researches have showed that high precision is always one of the most important goals in its development. In this paper, we systematically analyzed the disadvantages of Approximate Geometry Model (AGM) broadly adopt by InSAR. The AGM can not provide ideal level of precision because it does not take the curvature of the earth into account, assuming that the surface of the earth consists of planes. To achieve higher precision, we proposed Precise Geometry Model (PGM) which involves the curvature of the earth. The PGM has its obvious strengths especially when SAR images a wider area than it usually does. In fact, the precise model, to some extent, can prevent the errors which happen in each step from accumulating. It may decrease the possibility of total errors which affect the final output of InSAR. Based on the PGM, we proposed several significant steps of InSAR algorithms indicating how to flatten phase, estimate baseline and compute elevation for SAR interferometry. In addition, we implemented these steps in Visual Studio.Net and compared the experiment results with those obtained from commercial software such as EV-InSAR. Then we performed further analysis about results and reached a conclusion. Some suggestions were also be made for future research about PGM in more depth.

1. INTRODUCTION

Synthetic Aperture Radar Interferometry (InSAR), the synthesis of conventional SAR techniques and interferometry techniques, has been developed over several decades. Recently, InSAR has addressed several limitations in conventional SAR systems and been applied in numerous entirely new fields of earth science studies including detection of the earth's surface change, topographic mapping, classification of land cover and land cover [1].

The precision of DEM (Digital Elevation Model) derived from InSAR highly rely on several crucial steps of the processing which consist of the baseline estimation, flattening phase and elevation computation. Since each step has its own characteristics, we summarized the recent researches respectively as follows: First, the current approach for baseline estimation mostly roots in parameters from satellites which are used with geometric parameters from InSAR to obtain the baselines. Now that the current approach had been proven its conciseness and efficiency, we estimated baselines by a very familiar way with a slight difference. Second, flattening phase can be performed in both time domain and frequency domain. In the time domain, the output of phase times the minus ground phase is equal to that of frequency spectrum transfer after Fourier Transform. In the frequency domain, on the other hand, frequencies of brightest fringes in both azimuth and range directions are evaluated and then corresponding complements are made to counteract the ground phase effects. Finally, methods of elevation computation can be classified into two categories according to whether control points are needed. Most algorithms base on geometry model of InSAR which helps establish the parameter equations regardless of whether control points are involved. However, the geometry models of InSAR are almost Approximate Geometry Model (AGM), a simplified model at the expense of precision. Since we expected high precision of InSAR output, we proposed Precise Geometry Model (PGM) to improve its results by implementing several algorithms for each significant step mentioned above.

2. INSAR ALGORITHMS BASED ON PGM

As we mentioned above, to obtain DEM is an essential application of InSAR techniques. In this process, two SLCs (Single Look Complex) in which store the information of phases are needed with the standard format of CEOS (Committee of Earth Observing System). Besides the SAR images, this format can also provide information about obit, acquisition time of each line, incidence angle of central pixels in each line and so on.

2.1 Principle of InSAR

Total phase ϕ_{total} of every pixel in SAR images consists of phase ϕ_0 which represents the characters of land objects and phase ϕ_R which is determined by a two-way route. Assuming that time break between two SAR images is very short, phase ϕ_0 remains the same in each image. Interferogram can be attained by registration of two SAR images and multiplication of plural conjugate images, in which ϕ_0 is eliminated and the left information is only related to topography and other transmission conditions. Then we divided the topography phase ϕ into two parts which are respectively flat ground phase ϕ_{flat} and altitude phase ϕ_{alt} shown in Equ.1.

$$\begin{aligned} \phi_{total} &= \phi_0 + \phi_R \\ \phi &= \phi_{flat} + \phi_{alt} \end{aligned} \tag{1}$$

Fig.2 shows how the SAR sensor takes images twice to use interferometry techniques. In this figure, S_1 and S_2

respectively represent two positions of a SAR sensor where it takes images twice. The length of the baseline B is the distance between S_1 and S_2. The letter α stands for the angle between the baseline and horizontal line. The distance H is the length of line S_1O, R_e the earth's radius and θ the view angle when the sensor takes images of P at the position of S_1. Then we assumed r and $r+\Delta r$ separately represent two routes when the sensor takes images at S_1 and S_2. In this paper, we mainly discussed repeating orbit InSAR carried by satellites. Thus, the interference phase ϕ is presented by slant range difference Δr in Equ.2.

$$\phi = \frac{4\pi}{\lambda}\Delta r \tag{2}$$

Based on the information in Fig.2, we deduced two basic equations in the Precise Geometry Model (PGM). One is Slant Range Difference Equation and the other one is Phase Equation.

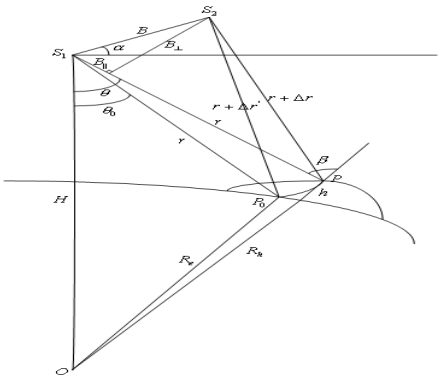

Fig.1 principle of InSAR

2.1.1 Slant Range Difference Equation

Because of the fact $\Delta r << r$, slant range difference Δr can be approximately presented by Equ.3 with neglect of Δr^2.

$$\Delta r = \frac{B^2}{2r} - B\sin(\theta-\alpha) \tag{3}$$

In the next step, we discussed whether the item $B^2/2r$ can be neglected in different conditions. According to Cycle Slicing Limit (CSL) proposed by Massonnet [2], the slant range error $\Delta\rho$ brought by noises should be controlled within the range of $\lambda/120$, namely $\Delta\rho < \lambda/120$. Then the item $B^2/2r$ can be eliminated from the equation. When SAR carrier is a plane, its conditions satisfy the CSL and we gained the Slant Range Difference Equation shown in Equ.4. However, when SAR carrier is a satellite, its conditions are not subjected to CSL and that item $B^2/2r$ should be maintained in Equ.5

$$\Delta r = -B\sin(\theta-\alpha) \tag{4}$$

$$\Delta r = \frac{B^2}{2r} - B\sin(\theta-\alpha) \tag{5}$$

2.1.2 Phase Equation

$$\theta-\theta_0 = arc\cos\left(\frac{r^2+H^2-R_h^{\,2}}{2rH}\right) - \arccos\left(\frac{r^2+H^2-R_e^{\,2}}{2rH}\right) \tag{6}$$

According to Equ.2 and Equ.5, we deduced the Phase Equation based on the geometric information from Fig.2. Then we gained the equation in Equ.6. From Equ.6 we knew that the value of $\theta-\theta_0$ is related to the height h at the position of P. Taking JERS Satellites as an example, we calculated parameters with known data ($r = 80000m$ and $H = 7151000m$) and reached conclusions as follows: When h = 6000 m, the value of $\theta-\theta_0$ is nearly one degree; when $h = 1000$ m, $\theta-\theta_0$ is about 0.173 degree. In consequence, higher positions accompany larger differences of view angles.

2.2 Algorithm for Flattening Phase

2.2.1 Principle of Flattening Phase

Since SAR directly stored the information of slant range, the phase recorded includes flat ground phase shown in Equ.1 which presents on the interferogram as periodical fringes under the name of "flat ground effect". During the process of InSAR, only the phase concerning altitude is expected and thereby flattening phase is a needed step for further processing. There are two major reasons that cause flat ground effect—baseline change along time and curvature of the earth. However, different ranges of images taken by SAR influence the result of flattening phase. While small scale of images can be flattened by simple linear method, wide images can not achieve satisfactory results unless curvature of the earth is taken into account. To obtain better output, we proposed an algorithm based on Precise Geometry Model for the step of flattening phase. According to Equ.5, Equ.6 and geometric information in Fig.2, the phase difference between P_1 and P_2 on the interferogram can be presented in Equ.7.

$$\Delta\phi_R = -\frac{2\pi B^2}{\lambda r_1^2}\Delta r - \frac{2\pi B_{\perp 1}(H^2-R_h^{\,2}-r_1^2)}{\lambda H r_1^2\sin\theta_1}\Delta r \tag{7}$$

2.2.2 Algorithm for Flattening Phase

Based on the principle mentioned above, algorithm for flattening phase can be described in details as follows. Assuming an image with the width of M (slant range direction) and length of N (azimuth direction), steps of the algorithm can be implemented in the following order.

1. Calculate basic parameters including B, α and H. (These letters are defined in chapter 2.1)
2. Calculate slant range of every point on the image according to nearest range r_{1st} and farthest range r_{last} shown in Equ.8.

$$r_j = r_{1st} + j\times\frac{r_{last}-r_{1st}}{N} \tag{8}$$

3. Compute the distance R_h between the image center and the earth's center with the data of incidence angle β and length of slant range $r_{N/2}$ at the image central point.
4. Compute θ_j by use of r_j according to Equ.9

$$\theta_j = \arccos\left(\frac{r_j^2 + H^2 - R_h^2}{2Hr_j}\right) \quad (9)$$

5. Compute the flat ground phase difference between column j and the central column N/2 in Equ.10

$$\Delta\phi_R^j = \frac{2\pi B\cos(\theta_{N/2}-\alpha)}{\lambda H\sin\theta_{N/2}}\Delta r_j - \frac{2\pi B^2\Delta r_j}{\lambda r_{N/2}^2} - \frac{4\pi B(H^2-R_h^2)\cos(\theta_{N/2}-\alpha)}{2\lambda H r_{N/2}^2\sin\theta_{N/2}}\Delta r_j \quad (10)$$

6. After some practical revision of Equ.10, flat ground phase of every point at the coordinate of (i, j) can be presented in Equ.11

$$\Delta\phi_R^{i,j} = \left(\frac{2\pi B\cos(\theta_{N/2}-\alpha)}{\lambda H\sin\theta_{N/2}} - \frac{2\pi B^2}{\lambda r_{N/2}^2} - \frac{4\pi B(H^2-R_h^2)\cos(\theta_{N/2}-\alpha)}{2\lambda H r_{N/2}^2\sin\theta_{N/2}}\right)\times(\Delta r_1 + K\times\Delta r_j) \quad (11)$$

7. To a point P(i, j), the result of flattening phase can be attained by phase recorded $\phi^{i,j}$ in a SAR image minus the flat ground phase $\Delta\phi_R^{i,j}$, namely $\phi_{topo} = \phi^{i,j} - \Delta\phi_R^{i,j}$
8. Observe the output of this step: if unsatisfactory result is gained, we should adjust some basic parameters and go back to reprocess it; otherwise, we need only store it for next steps

2.3 Algorithm for Elevation Computation

2.3.1 Principle of Elevation Computation

With the assumption of no noises, the left information of interferogram after flattening phase merely reflects elevation. However, it can not be directly applied to compute elevation because the phase recorded on intergerogram is only a part of its real value called major value with a range of $(-\pi, \pi]$. The real value of a phase is equal to its major value plus integral multiple of 2π, in a process call phase unwrapping [3]. After establishing the relation between the real phase difference $\Delta\phi_Z$ and the elevation Δz as shown in Equ.11, interferogram can be used to produce DEM by elevation computation.

$$\Delta\phi_Z = -\frac{4\pi B\cos(\theta_0-\alpha)R_h}{\lambda r_0 H\sin\theta_0}\Delta z \quad (11)$$

2.3.2 Algorithm for Elevation Computation

Based on the geometric information in Fig.2 and algebraic relation in Equ.11, we proposed an algorithm for elevation computation shown in Fig.4. This algorithm grounded on Price Geometry Model (PGM) brings improved ambiguity of height in Equ.12 compared to those of Approximate Geometry Model (AGM) in Equ.13. While two equations have the same value only at image central point, the ambiguity of height rooting in PGM which involves curvature of the earth has better precision at other points.

$$\Delta z_{2\pi} = -\frac{\lambda r H\sin\theta}{2B\cos(\theta-\alpha)R_h} \quad (12)$$

$$\Delta z'_{2\pi} = -\frac{\lambda r\sin\theta_0}{2B_\perp} \quad (13)$$

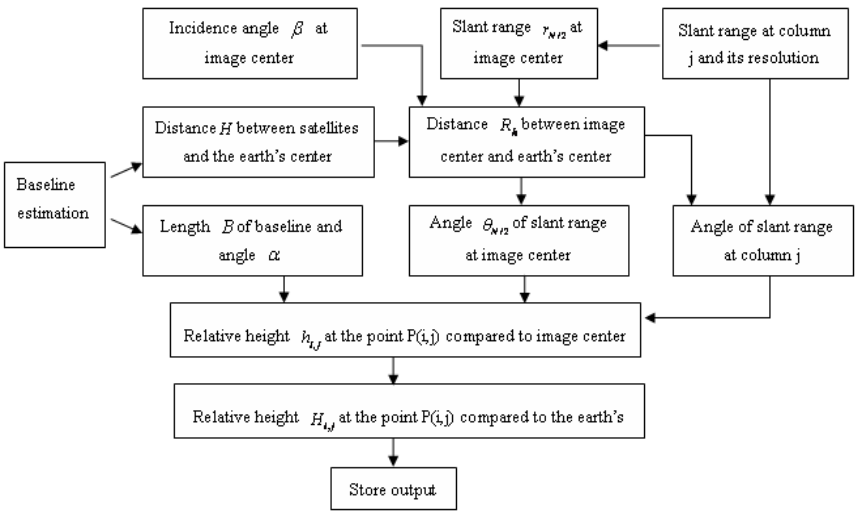

Fig.2 flow chart of algorithm for elevation computation

2.4 Algorithm for Baseline Estimation

As shown in Fig. 4, there are five vector points on the master track including P_{m1} P_{m2} P_{m3} P_{m4} P_{m5} which are separately corresponding to its UTM time t_{m1} t_{m2} t_{m3} t_{m4} t_{m5}. Similarly,

P_{s1} P_{s2} P_{s3} P_{s4} P_{s5} represent five vector points on the slave track with separate UTM time t_{s1} t_{s2} t_{s3} t_{s4} t_{s5}.

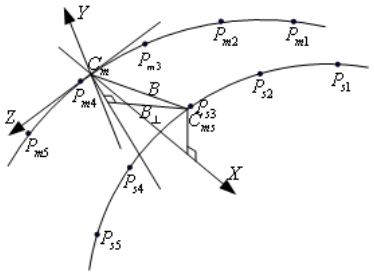

Fig.3 InSAR special information map

The track point C_m stands for the center of master image with its time t_{cm} and C_{ms} the center of slave image with its time t_{cs}. In the practical baseline estimation, we must obtain the parameters of points C_m and C_{ms}. And then the length of baseline B can be calculated by the distance between points C_m and C_{ms}. Equ.14 shows this process.

$$\begin{aligned} \vec{C}_{ms} &= (\vec{X}_s(t_{cms}), \vec{Y}_s(t_{cms}), \vec{Z}_s(t_{cms})) \\ \vec{C}_m &= (\vec{X}_m(t_{cm}), \vec{Y}_m(t_{cm}), \vec{Z}_m(t_{cm})) \\ B &= \vec{C}_{ms} - \vec{C}_m \end{aligned} \tag{14}$$

There are two major methods of baseline estimation [4]. They both root in a fact that the projective value of B on the Z axis is zero, namely $B_z = 0$. The function extremum method expects the least value of $|\vec{B}|$. When the equ.15 reaches its least value, this value is the length of baseline. The vector method considers the speed of satellites at the point C_m as a vector. Then the restraint condition is converted into Equ.16.

$$|B|^2 = \left(a_{s0} + a_{s1}t + a_{s2}t^2 + a_{s3}t^3 - X_m(t_{cm})\right)^2 + \left(b_{s0} + b_{s1}t + b_{s2}t^2 + b_{s3}t^3 - Y_m(t_{cm})\right)^2 + \left(c_{s0} + c_{s1}t + c_{s2}t^2 + c_{s3}t^3 - Z_m(t_{cm})\right)^2 \tag{15}$$

$$\vec{V} \cdot \vec{B} = \vec{V} \cdot (\vec{C}_{ms} - \vec{C}_m) = 0 \tag{16}$$

3. EXPERIMENT AND ANALYSIS

We used a pair of SAR images obtained from JERS-1 SAR sensor to examine algorithms for baseline estimation, flattening phase and elevation computation. First, we simulated master and slave tracks by information stored in SAR images to obtain parameters of baselines. The result we obtained was compared with that of commercial software EV-InSAR as shown in Tab.1.

Second, we applied the algorithm based on PCM for flattening phase to the raw interferogram. Then we compared the output with that of method from ACM as illustrated in Fig.4. Third, the step of elevation computation was implemented in three ways including algorithm based on PCM, method from ACM and EV-InSAR. Three results were discussed in details shown in Fig.5.

method	Length of baseline (m)	Horizontal baseline (m)	Vertical baseline (m)
algorithm based on PCM	1115.2398205	1034.679468	416.170847
EV-InSAR	1115.378919	1036.43479826	412.156574423

Tab.1 comparison of baseline estimation

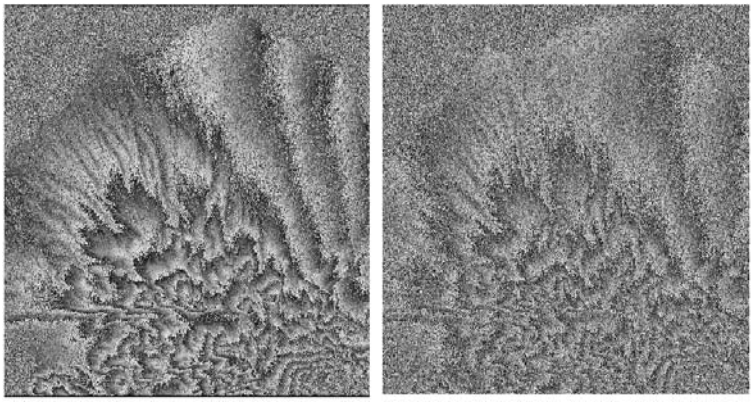

Fig.4 output of flattening phase, the left one is the result of algorithm based on PGM and the right is output of AGM

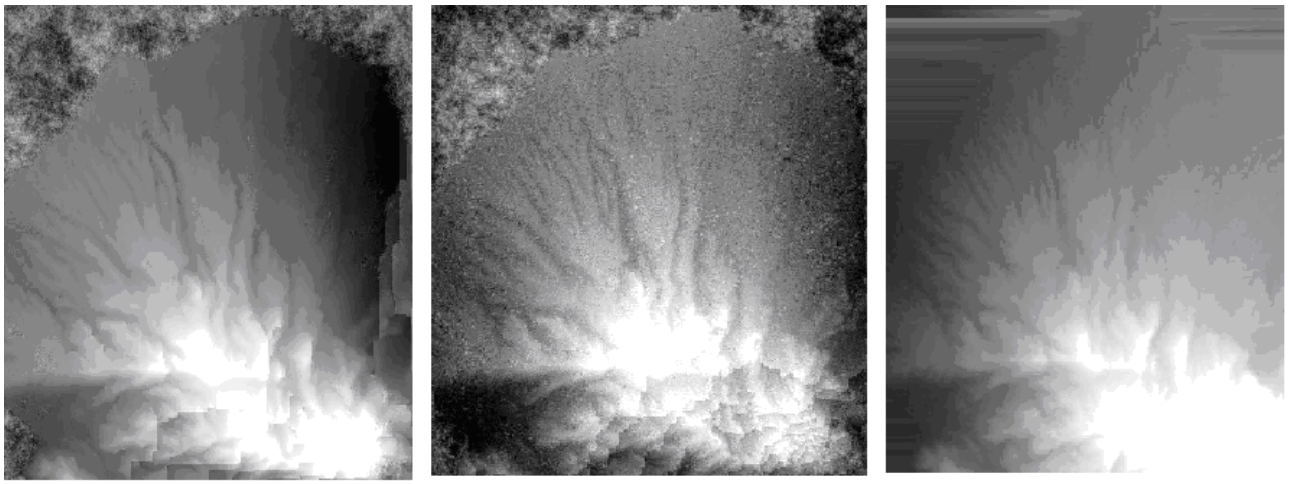

Fig.5 results of three methods for elevation computation
5(a) represents algorithm based on PGM; 5(b) stands for method of AGM; 5(c) is the output of EV-InSAR

Assuming that J_DEM data reflected the real elevation of this area, we used this data to examine precision of different methods. After randomly choosing 100 points, we compared errors in three DEM. However, the errors in DEM are not satisfactory regardless of which method is used. In consequence, we knew that introduction of Control Points (CPs) is a must. We separately established quadratic and cubic polynomials by using different number of control points summarized in Tab.2. We reached a conclusion that more CPs brings better precision.

Classification of elevation computation	dMax (m)	dMin (m)	dMean (m)	dStd (m)
Quadratic polynomial (8CPs)	-62.953526	0.396539	2.155458	29.704037
Quadratic polynomial (16CPs)	-38.400963	0.163755	2.351149	11.341672
Cubic polynomial (16CPs)	-32.556606	-0.140959	2.323029	11.253101

Tab. 2 outputs of three polynomials by using control points

4. CONCLUSION

This paper has systematically analyzed the disadvantages of Approximate Geometry Model (AGM). To achieve higher precision especially when SAR images a wider area than it usually does, we proposed Precise Geometry Model (PGM) to develop algorithms of flattening phase, baseline estimation and elevation computation for SAR interferometry. In addition, we implemented these steps in Visual Studio.Net and compared the experiment results among different approaches. Then we proposed a method of elevation revision by utilizing polynomials and control points. Some suggestions were also be made for future research on PGM in more depth.

REFERENCES

[1] Paul A. Rosen, Scott Hensley, Ian R. Joughin, Fuk K. Li, Soren N. Madsen, Ernesto Rodriguez, Richard M. Goldstein, 2000. Synthetic aperture radar interferometry. Proceedings of the IEEE, 88(3), pp 333-381

[2] Massonnet D., Rossi M, Carnoma C., 1993. The displacement field of the landers earthquake mapped by rader interferometry. Nature, 36(4), pp 138-142

[3] Goldstein R. M., Zebker H. A., Werner C. L, 1998. Satellite radar interferometry: two-dimensional phase unwrapping. Radio Science, 23(4), pp 4993-4999

[4] Zheng Fang, Wu Junting, Ma Debao, 2005. Baseline estimation based on track errors and elevation precision images. Proceeding of the Information Engineering Univeristy, 6(1), pp 77-79